DAILY QA
Finished before your first cup of coffee

MONTHLY QA
Never re-learn workflow again

ANNUAL QA
Confidence with fewer gray hairs

STEREOTACTIC
When millimeters matter most

ABSOLUTE DOSIMETRY
"Pinpoint" is our margin of error

PATIENT DOSIMETRY
Pre-treatment is just the beginning

QA Solutions. ***Our expertise is at your service.***

STANDARD IMAGING®

MORE THAN JUST QA PRODUCTS, FIND QA SOLUTIONS AT

www.standardimaging.com

1411-00, 2/18

NMR blood flow imaging using multiecho, phase contrast sequences

M. O'Donnell
Corporate Research & Development Center, General Electric Company, Schenectady, New York 12301

(Received 13 March 1984; accepted for publication 4 June 1984)

Moving nuclei, in contrast to stationary nuclei, experience a phase shift in the presence of a balanced gradient. Monitoring of this phase shift can be used to measure the flow velocity of moving nuclei. A specific scan sequence for blood flow imaging is presented. This sequence uses multiple echoes as well as a phase contrast approach to generate both conventional anatomical images and blood flow images from the same data. Images of a phantom and a human volunteer demonstrating the accuracy of the method are presented.

I. INTRODUCTION

Since the 1950s nuclear magnetic resonance (NMR) has been used to monitor the velocity of flowing fluids. Review articles by Singer and by Jones and Child cover the major contributions to NMR flow measurements.[1,2] In recent years, several investigators have attempted to merge these flow measurement techniques into NMR imaging pulse sequences to generate quantitative blood flow images. Most of the methods proposed to date use selective irradiation to "tag" protons so that the pixel brightness in an NMR image is related to the velocity of the flowing protons.[3–10] In essence, all these methods use the signal amplitude to measure the replacement of saturated or partially saturated protons by unsaturated protons. Although conceptually simple, these methods are fraught with difficulties since there are many factors besides flow velocity that can influence the pixel brightness in a conventional NMR image. Indeed, Crooks *et al.* note that the signal amplitude in a flowing region is intimately linked to the particular pulse sequence used for imaging.[9]

An alternative method for measuring flow using NMR monitors the phase of the NMR signal after the application of pulsed gradients. In particular, the pulsed gradients are chosen such that the phase of stationary objects is not changed but the phase of moving objects is altered in simple proportion to the velocity. This method was first proposed by Hahn in 1960 to detect the motion of seawater.[11] In the last few years several authors have attempted to incorporate a pulsed gradient scheme for flow encoding into conventional imaging sequences.[12,13] This paper presents an efficient method for flow imaging using pulsed gradients and the principle of phase contrast. The technique presented here permits simultaneous generation of conventional NMR amplitude images and phase contrast flow images from the same data set.

II. METHODS

Measuring fluid flow using pulsed gradients was first proposed by Hahn who noted that flowing nuclei experience a phase shift in the presence of a balanced gradient (i.e., a gradient pulse with zero mean over a finite time).[11] Two balanced gradient sequences for measuring flow along the axis of the gradient are presented in Fig. 1. These sequences alter the phase in precisely the same way because the 180° pulse in Fig. 1(a) inverts the phase rotation produced by the first gradient pulse, thus generating a phase rotation equivalent to the inverted gradient pulse in Fig. 1(b).

The phase rotation introduced by any gradient sequence is given by the expression

$$\phi = \int_0^\tau \gamma G(t)\, z(t)\, dt, \tag{1}$$

where γ is the gyromagnetic ratio for the nuclei under investigation, τ is the duration of the gradient pulse, and we assume that the gradient pulse $G(t)$ is applied along the z axis. For the pulse sequence presented in Fig. 1, Eq. (1) becomes

$$\phi = \gamma G\left[-\int_0^\tau z(t)dt + \int_\tau^{2\tau} z(t)dt \right], \tag{2}$$

where G is the magnitude of the gradient pulse. Of course, for stationary nuclei Eq. (2) reduces to zero, and hence there is no net phase rotation. However, if nuclei are moving in the z direction with a uniform velocity v over the duration of the gradient pulse, then the phase rotation becomes

$$\begin{aligned}\phi &= \gamma G v[-\tau^2/2 + 2\tau^2 - \tau^2/2] \\ &= \gamma G v \tau^2 .\end{aligned} \tag{3}$$

That is, the phase rotation of uniformly flowing nuclei is independent of position and is proportional only to the flow velocity, the magnitude of the applied gradient, and the square of the duration of each lobe of the flow encoding pulse. Also, the sign of the phase change is determined by the direction of the flow relative to the gradient direction. Thus, for the gradient sequences presented in Fig. 1, flow in the

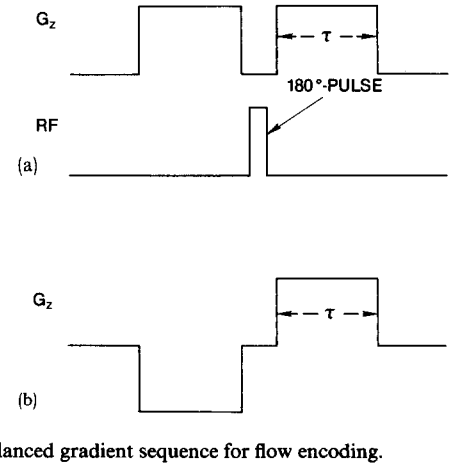

FIG. 1. Balanced gradient sequence for flow encoding.

 0094-2405/85/010059-06$01.20

direction of the gradient generates a phase advance, whereas flow antiparallel to the direction of the gradient generates a phase retardation.

The simple expression presented in Eq. (3) is the basis for the specific method presented in this paper, as well as for the method proposed by Moran.[12] Moran incorporates a flow encoding pulse into an imaging sequence just prior to the onset of the spin echo used for conventional imaging (i.e., just prior to the onset of the readout gradient). In this approach, the magnitude of the flow encoding pulse is swept over a range of values spaced evenly between some maximum and minimum amplitudes. Such a gradient sequence serves to encode the spins for flow velocity in analogy to the phase encoding used for spatial localization in spin-warp imaging. At each value of the flow encoding pulse, a standard imaging sequence is completed and an image is generated using conventional reconstruction methods. That is, N independent images are obtained corresponding to the N independent values of the flow encoding pulse. This set of images is then Fourier transformed with respect to the flow encoding sequence on a pixel by pixel basis to generate a set of N flow images. Each image of this set displays all pixels within the object moving with a particular flow velocity, where the pixel brightness is determined by either the spin density or the relaxation times in that pixel. Although conceptually appealing, this method exhibits limited dynamic range since the velocity resolution is determined by the number N of independent flow encoding pulses.

An alternate approach to flow imaging is to use the principle of phase contrast in conjunction with the pulsed gradient scheme for flow encoding. The basis of the phase contrast method is to switch a fixed flow encoding pulse on and off at each value of the imaging gradients. In the particular method used in this study, the flow encoding pulse is applied after the phase encoding pulse (pulses) and just prior to the readout gradient of a modified spin-warp imaging sequence.[14] The flow encoding pulse is strobed on and off on each successive repetition interval of the spin-warp sequence, and data is acquired both when the flow encoding pulse is on and when it is off (see Fig. 2, where we note that data is acquired only during the readout interval of the x gradient). Two images can then be formed; the first is the image generated from data obtained in the absence of flow encoding and the second is the image obtained from data acquired with flow encoding. The first image is a conventional image, where the reconstruction consists of Fourier transforming the spin-echo data in three dimensions (or two dimensions) to yield

$$A_1(x, y, z) = \rho'(x, y, z) e^{i\phi(x, y, z)}. \tag{4}$$

In Eq. (4), $A_1(x, y, z)$ is the complex value at each pixel (x, y, z) obtained from the 3D Fourier transform of the data, $\rho'(x, y, z)$ is the spin density, or the spin density modified by the relaxation times, and $\phi(x, y, z)$ is a phase factor which may vary throughout the image plane. The phase term, $\phi(x, y, z)$, can be nonzero for many reasons. For example, if the rf field

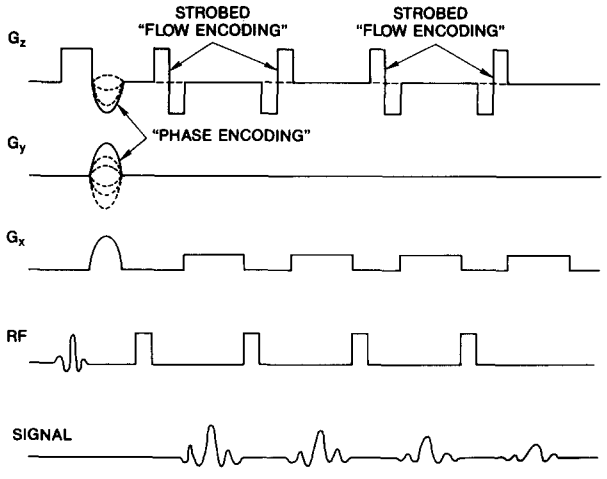

FIG. 2. Pulse sequence for multiecho, phase contrast imaging.

used to excite the spins generates eddy currents within the body, then the phase of the exciting rf field may vary throughout the image plane. To overcome the effects of phase variations throughout the image plane, the modulus of A, $|A(x, y, z)|$, is usually displayed so that an unambiguous representation of $\rho'(x, y, z)$ is presented. Indeed, the modulus of $A(x, y, z)$ represents a conventional NMR image. However, for the phase contrast method of flow imaging, the entire complex number, $A_1(x, y, z)$, must be retained.

Because the same flow encoding pulse shape is used throughout the entire imaging sequence, the spin-echo data obtained when the flow encoding pulse is applied represent the spatial Fourier transform of the density function modulated in phase by the magnitude of flow within each pixel as well as by the phase term $\phi(x, y, z)$. A second image can be obtained from these data simply by performing the 3D Fourier transform, as was done for data acquired in the absence of flow encoding. For example, if a flow encoding pulse of magnitude G and duration τ is applied along the z direction, then the reconstructed complex value at each pixel for the second image is

$$A_2(x, y, z) = \rho'(x, y, z) e^{i\gamma G v_z(x, y, z)\tau^2} e^{i\phi(x, y, z)}. \tag{5}$$

In Eq. (5) $v_z(x, y, z)$ is the component of the flow velocity along the z axis at position (x, y, z). Note that the magnitude representation [i.e., $|A(x, y, z)|$] is identical for the two images. The only difference between the two images given by Eqs. (4) and (5) is that the phase in each pixel of the second image is rotated with respect to the phase of the first image in proportion to the flow velocity in each pixel. In pixels where there is no flow, both the magnitude and phase of the two images are identical. As a consequence, the phase difference between $A_2(x, y, z)$ and $A_1(x, y, z)$ generates an image that is directly related to the flow velocity in each pixel and is independent of phase variations unrelated to flow. This phase contrast image is computed using the expression

$$\Delta\phi(x, y, z) = \tan^{-1}\left[\frac{\mathrm{Im}\,A_2(x, y, z)\,\mathrm{Re}\,A_1(x, y, z) - \mathrm{Re}\,A_2(x, y, z)\,\mathrm{Im}\,A_1(x, y, z)}{\mathrm{Re}\,A_1(x, y, z)\,\mathrm{Re}\,A_2(x, y, z) + \mathrm{Im}\,A_1(x, y, z)\,\mathrm{Im}\,A_2(x, y, z)}\right], \tag{6}$$

and is related to the flow velocity by

$$\Delta\phi\,(x, y, z) = \gamma G v_z\,(x, y, z)\tau^2. \tag{7}$$

Finally, we can obtain a flow image from the phase contrast image by inverting Eq. (7)

$$v_z\,(x, y, z) = \frac{\Delta\phi\,(x, y, z)}{\gamma G \tau^2}. \tag{8}$$

The use of phase contrast greatly reduces the data acquisition time for quantitative flow imaging since only one additional repetition of the entire imaging sequence is needed to obtain flow information. Thus, only 2 min are needed to acquire all the data for reconstruction of the flow velocity along a particular axis if the conventional imaging sequence takes 1 min. Similarly, a complete reconstruction of both the magnitude and direction of the flow takes 4 min for a 1 min imaging sequence. Although these times are quite reasonable for most clinical applications, there is one problem inherent to the phase contrast approach that must be remedied before it can be used routinely in the clinic.

The phase, or phase difference, is a periodic function uniquely defined only over the range $-\pi$ to π. Thus, if the flow velocity in a particular pixel creates a phase advance (retardation) greater than π, then the reconstruction algorithm for flow imaging presented in Eqs. (7) and (8) will compute the wrong value for the flow velocity. This, of course, is just the classic aliasing problem for a periodic function. To overcome this problem, the magnitude and duration of the flow encoding pulse is chosen to satisfy the Nyquist criterion. That is, the gradient is chosen such that the maximum flow velocity expected generates a π radian phase change. To ensure that all flow velocities are faithfully reproduced, the maximum flow velocity must be chosen conservatively. This means that many of the velocities of interest may produce very small phase changes. Small phase changes are difficult to measure since the electrical noise in the imaging system introduces a random phase component superimposed on the actual phase change. Thus, the minimum flow velocity measurable, as well as the velocity resolution, is determined by the signal-to-noise ratio. For many applications, especially measurements of flow velocity with high spatial resolution, the dynamic range in flow velocities imposed by these restrictions may prove too small to be useful.

To increase the dynamic range and the velocity resolution in measurement of flow without paying a significant penalty in time, the phase contrast method described above can be incorporated into a multiecho imaging sequence. A complete phase contrast image is generated for each echo such that

$$\Delta\phi_n\,(x, y, z) = (-1)^{n-1}\, n[\gamma G v_z\,(x, y, z)\tau^2], \tag{9}$$

where n is the echo index. In Fig. 2 a complete pulse sequence for 3D multiecho, phase contrast imaging is presented. The sequence given in this figure images flow along the z axis, but it can be easily generalized for imaging along any axis or for imaging of both the magnitude and direction of the flow. Note that all flow encoding pulses are alternately turned off and on for each value of the phase encoding gradients. Also, note that the polarity of the flow encoding pulse is inverted from echo to echo. This polarity reversal is used to counteract the phase inversion produced by the 180° pulse so that the phase change introduced by each flow encoding pulse adds to the phase change introduced by previous flow encoding pulses [Eq. (9)].

The flow image generated by this sequence is reconstructed by first plotting the phase, after correction for the sign reversal [i.e., multiple $\Delta\phi_n\,(x, y, z)$ by $(-1)^{n-1}$] as a function of echo number. For velocities near the Nyquist rate, the cumulative phase may be aliased on certain echoes. However, because there is no aliasing on a single echo, the phase difference can be unwrapped as a function of echo number for all velocities satisfying the Nyquist criterion. Following phase unwrap, the phase difference is fit to a straight line as a function of echo number. The slope of this fit represents the average phase rotation per echo and is related to the flow velocity by

$$v_z\,(x, y, z) = \bar{\phi}\,(x, y, z)/(\gamma G \tau^2), \tag{10}$$

where $\bar{\phi}\,(x, y, z)$ is the slope. This processing serves to increase the dynamic range by reducing the effect of noise. In particular, if all the echoes are recorded in a time less than the T_2 of blood, then the dynamic range is increased approximately by the square root of the number of echoes. Since the T_2 of blood is greater than 200 ms, four to six echoes can be recorded in a time well less than the T_2 of blood. Thus, the multiple echo method can easily increase both the dynamic range and the velocity resolution of the phase contrast approach by a factor of about 2 to 2.5. In the next section we present the results of a preliminary investigation of the multiple-echo, phase contrast method.

III. RESULTS

As an initial test of the method presented in the previous section, both amplitude and phase contrast images of a flow phantom were generated. The flow phantom consists of eight tubes of four different sizes (6.4, 9.5, 12.7 and 15.9 mm in diameter). The tubes are connected in series and the flow through the phantom is controlled such that for each size there is forward flow in one tube and reverse flow in the other. The length of the tubes is sufficiently long to ensure nearly Laminar flow (i.e., nonturbulent flow) under all con-

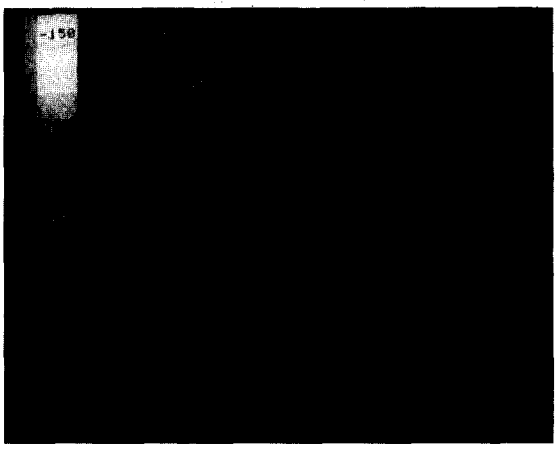

FIG. 3. Amplitude image of flow phantom in the absence of flow (top panel) and the presence of flow (bottom panel).

ditions. Continuous flow through the phantom is maintained with a mechanical pump. Because the tubes are connected in series and nonturbulent flow is present, the average flow velocity in each tube varies simply as the inverse of the cross-sectional area of the tube.

The phantom was positioned inside the bore of the magnet such that the direction of flow within the phantom was either parallel or antiparallel to the direction of the main magnetic field (z axis). The phantom was imaged using a 2D, partial saturation, multiple-echo, phase contrast sequence sensitive only to flow along the z axis (i.e., the sequence of Fig. 2 with flow encoding along the z axis but without phase encoding along the z axis). All images presented in this paper were obtained at a field strength of approximately 0.15 T using an experimental whole-body scanner developed in our laboratory. A two-echo sequence was used for all images. In Fig. 3 the amplitude image of the phantom for a flow rate of 400 cm^3/min is presented in the lower panel and the image generated when the flow pump was turned off is presented in the upper panel. These images were obtained by first averaging the magnitude images at each echo for flow encoding on and flow encoding off {i.e.,

$$A(x, y) = [|A_1(x, y)| + |A_2(x, y)|]/2\}.$$

In general, the average magnitude image at each echo can be handled as if it was the magnitude image in a conventional multiple-echo sequence. Thus, T_2 images as well as more conventional amplitude images can also be generated from the data. However, in this study all amplitude images, including Fig. 3, were obtained simply by averaging the images from both echoes. In Fig. 4 the phase contrast images generated from the same data are presented. The grey scale in these images is defined such that zero flow corresponds to a value of zero and an intermediated grey level. Flow into the plane of the image is represented by a value greater than zero and a grey level brighter than the median grey. Similarly, flow out of the plane of the image is represented by a value less than zero and a grey level darker than the median grey. In Fig. 5 the flow distribution within one of the tubes is presented, where the ordinate in this figure is the flow velocity scaled to the maximum flow in the tube. As is evident

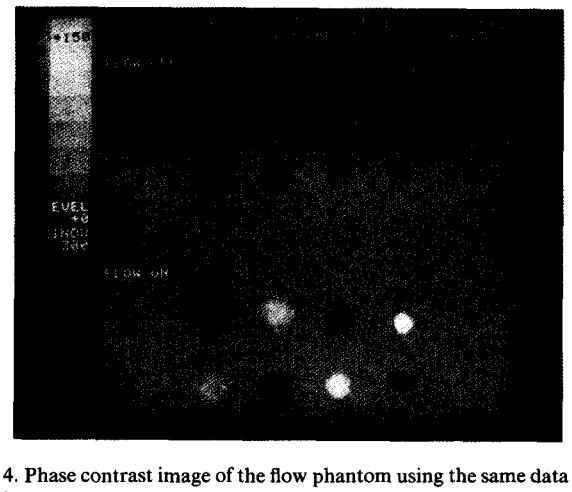

FIG. 4. Phase contrast image of the flow phantom using the same data as in Fig. 3.

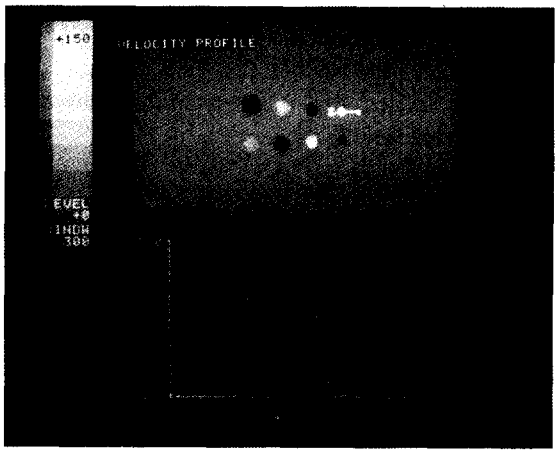

FIG. 5. Flow distribution within one of the tubes of the phantom.

from these figures, the multi-echo, phase contrast method is able to image both the magnitude and the direction of the flow velocity in the phantom.

To test the quantitative accuracy of the method, the average velocity and the standard deviation of the velocity were computed within each of the eight tubes. The results are summarized in Fig. 6, where the results for flow into the plane of the image are presented in Fig. 6(a) and the results

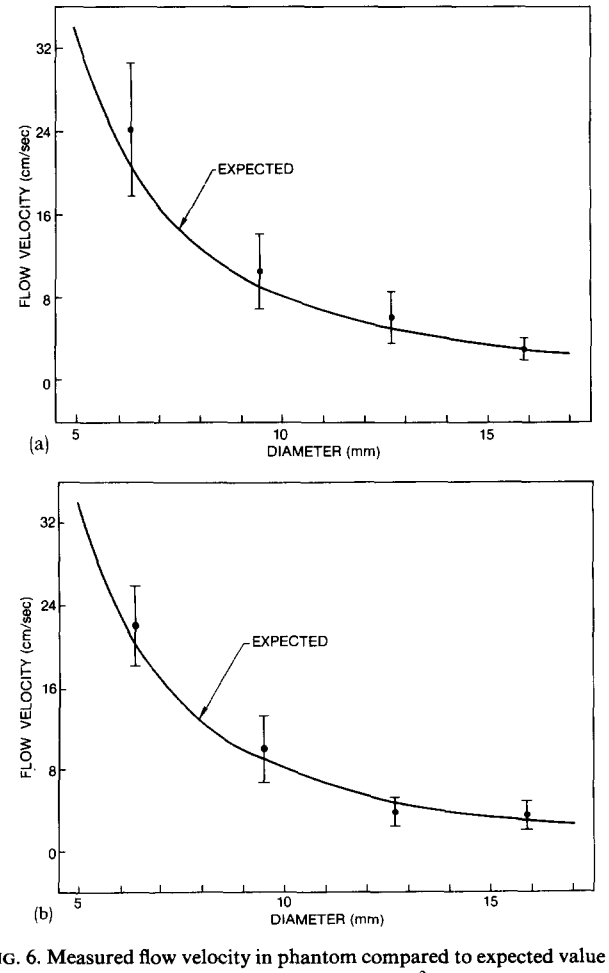

FIG. 6. Measured flow velocity in phantom compared to expected value for both (a) forward flow and (b) reverse flow. 400 cm^3/min.

FIG. 7. Amplitude image of volunteer in the abdominal region.

for flow out of the image plane are presented in Fig. 6(b). The solid curve in this figure is the average flow velocity expected as a function of the tube diameter assuming Laminar flow for a volume flow rate of 400 cm^3/min. Of course, because the tubes are connected in series, the average velocity should vary as the inverse square of tube diameter for nonturbulent flow. Also, the standard deviaton should scale proportionately with the average velocity for near-Laminar flow. An inspection of the results presented in Fig. 6 clearly demonstrates the quantitative accuracy of the method. The measured mean velocity very closely parallels predicted results for both flow directions. In addition, the standard deviation scales with mean flow velocity as predicted.

As a further test of the method, multiple-echo phase contrast images of a healthy, adult volunteer were obtained. The results for a simple 2D, two-echo sequence are presented in Figs. 7 and 8. The image shown in Fig. 7 is the amplitude image of an axial slice in the abdominal region. The volunteer's right-hand side is the left-hand side of the image. Data acquisition for this image took 1.5 min, with a pixel dimension of 3.5 mm and a slice thickness of 1 cm. Again, this image was obtained at 0.15 T. The phase contrast image generated from the same data set is presented in Fig. 8, where the display has been clipped to ensure that the flow velocity

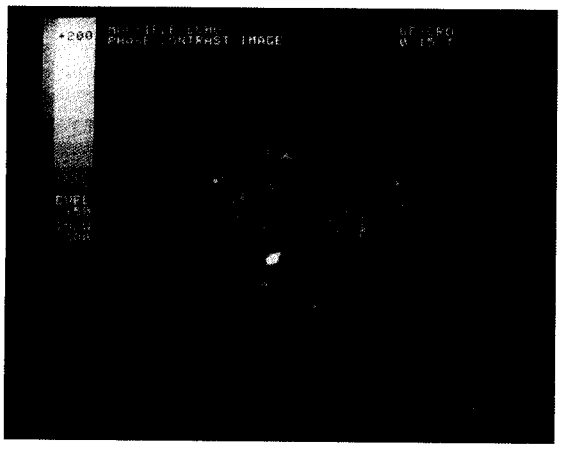

FIG. 8. Phase contrast image of volunteer in the abdominal region.

is displayed only in those pixels with an amplitude above a certain threshold value (i.e., the flow velocity is displayed only in those pixels where there is sufficient signal to ensure an accurate phase measurement). In Fig. 8 the abdominal aorta and the inferior vena cava are clearly visible, where the blood in the vena cava is correctly depicted as flowing into the plane of the image and the blood in the aorta is correctly depicted as flowing out of the plane of the image.

The average value of the flow velocity in the vena cava is 10.5 ± 5.4 cm/s (peak velocity equals 19.6 cm/s), a value well within the normal range for a healthy adult at this level of the abdomen. We note that the standard deviation in the flow velocity is directly related to the flow distribution in the artery and not to measurement errors. The velocity resolution in this image is significantly better than 0.5 cm/s. The average value of the velocity in the aorta is only -8.1 ± 2.4 cm/s (peak velocity equals -12.4 cm/s), a value smaller than the expected average in a healthy adult. The reason for this underestimate is related to the pulsatile nature of flow in the major arteries. During the interval of the cardiac cycle where peak flow is present in the aorta, the phase was aliased for the flow encoding pulse used in this experiment. The amplitude of the flow encoding pulse was chosen to produce substantial phase shifts for the average flow velocities in the vena cava and the aorta. During the interval of low flow, the phase was faithfully measured. Because these measurements were not synchronized with the cardiac cycle, the aliased measurements averaged with the good measurements result in an underestimation of the true phase change associated with flow in the aorta. This problem can be circumvented by insuring that the gradients are chosen such that peak flow in the major arteries is not aliased. Nevertheless, the results presented in Figs. 7 and 8 clearly demonstrate the utility of the multiple-echo, phase contrast approach.

IV. DISCUSSION

Quantitative measurement of the flow velocities in vessels may prove to be an extremely useful tool for the assessment and monitoring of impaired flow due to arterial disease. In this paper a flow imaging sequence based on the principle of phase contrast has been presented. In addition, this sequence exploits multiple echoes to enhance the dynamic range and the resolution of the velocity measurement. The results presented in Figs. 3–8 clearly demonstrate that the method can be used to accurately image the magnitude and direction of continuous flow over a large dynamic range with very fine velocity resolution. Unlike amplitude methods for flow imaging, a conventional image is also generated from the same data permitting precise anatomical identification of all regions of flow. Moreover, the specific sequence presented in Fig. 2 is efficient since the imaging time for measurement of blood flow along one axis is only two times the normal imaging time and for measurement of both magnitude and direction of blood flow is only four times the normal imaging time. This high efficiency at high-velocity resolution is the principal benefit of the specific method presented in this paper compared to other pulsed gradient methods.[12,13]

Although the results on continuous flow were quite accurate, measurement of pulsatile flow in this study was not

correct. This problem can be circumvented by insuring that peak flow components are not aliased. However, care must be taken in analyzing measurements of pulsatile flow. In particular, the dynamic range of the flow measurement must be chosen such that the peak velocities are not aliased and the minimum velocities are faithfully measured above the noise. Choosing the dynamic range in this way ensures that the flow image truly represents the temporal average of the flow in the artery if all intervals during the cardiac cycle are equally sampled. Another approach to measuring pulsatile flow is to synchronize the imaging sequence with the cardiac cycle. In this way, the image represents a snapshot of the flow distribution at one point in the cardiac cycle. In any event, NMR methods for measuring blood flow, although potentially quite accurate, are not dynamic. Only temporal averages or snapshots at several points in the cardiac cycle can be obtained in reasonable imaging times. Accurate information on average flow distribution, however, should prove very useful for a number of clinical applications.

In addition to blood flow measurements, the pulse sequence presented in Fig. 2 can also be used to estimate diffusion constants. Tanner and Stejskal showed that a gradient sequence similar to the flow encoding pulses of Fig. 1 can be used to measure self-diffusion constants.[15] Using the notation developed in Sec. II, where diffusion effects are now explicitly included, the diffusion constant at any point x, y, z is given by the expression

$$D_n(x,y,z) = (3/2n\gamma^2\tau^3G^2)\ln\left(\frac{|A_1(x,y,z)|}{|A_2(x,y,z)|}\right), \qquad (11)$$

where $D_n(x,y,z)$ is the estimate of the diffusion constant for the nth echo. The measurements of $D_n(x,y,z)$ for each echo can then be averaged to generate an estimate of the diffusion constant. It is not clear whether measurement of diffusion constants generally may yield additional information of clinical relevance. However, measurement of diffusion constants may prove useful in monitoring perfusion of organs in which there is negligible directional flow over the duration of the imaging sequence. In any event, the multiple-echo, phase contrast sequence is a very efficient approach permitting the simultaneous computation of conventional images, such as partial saturation and T_2 images, as well as blood flow images and diffusion constant images from the same data set.

ACKNOWLEDGMENTS

S. G. Karr, G. Brower, and J. M Wang were responsible for constructing the flow phantom. Helpful discussions with H. R. Hart on early drafts of the manuscript are gratefully acknowledged. Also, general comments by our local kibitzer, W. A. Edelstein, are appreciated. E. M. Engler was responsible for production of the manuscript.

[1]J. R. Singer, J. Phys. E **11,** 281 (1978).
[2]D. W. Jones and T. F. Child, Adv. Magn. Reson. **8,** 123 (1976).
[3]J. R. Singer, Science **130,** 1652 (1959).
[4]J. H. Battocletti, R. E. Halbach, S. X. Salles-Cunha, and A. Sauces, Jr., Med. Phys. **8,** 435 (1981).
[5]R. E. Halbach, J. H. Battocletti, S. X. Salles-Cunha, and A. Sauces, Jr., Med Phys. **8,** 444 (1983).
[6]K. R. Thulborn, J. C. Waterton, P. Styles, and G. K. Radda, Biochem. Soc. Trans. **9,** 233 (1981).
[7]A. N. Garroway, J. Phys. D **7,** L159 (1974).
[8]J. R. Singer, IEEE Trans. Nucl. Sci. **27,** 1245 (1980).
[9]L. Crooks, P. Sheldon, L. Kaufman, and W. Rowan, IEEE Trans. Nucl. Sci. **29,** 1181 (1982).
[10]J. R. Singer and L. E. Crooks, Science **221,** 654 (1983).
[11]E. L. Hahn, J. Geophys. Res. **65,** 776 (1960).
[12]P. R. Moran, Magn. Reson. Imaging **1,** 197 (1982).
[13]D. A. Feinberg, in Proceedings of the 2nd Annual Meeting of the Society of Magnetic Resonance in Medicine (1983), p. 128.
[14]W. A. Edelstein, P. A. Bottomley, H. R. Hart, W. M. Leue, J. S. Schenck, and R. W. Redington, in Proceedings of an International Symposium on NMR Imaging, 1981.
[15]J. E. Tanner and E. O. Stejskal, J. Chem. Phys. **49,** 1768 (1968).